Available online at www.sciencedirect.com
SCIENCE DIRECT®
Chemometrics and Intelligent Laboratory Systems 66 (2003) 141–158
Chemometrics and intelligent laboratory systems
www.elsevier.com/locate/chemolab

Multi-way methods in image analysis—relationships and applications

Jun Huang[a,*], Helle Wium[b], Karsten B. Qvist[b], Kim H. Esbensen[c]

[a] *PerkinElmer Instruments, 710 Bridgeport Avenue, Shelton, CT 06484, USA*
[b] *Department of Dairy and Food Science, and Centre for Advanced Food Studies, The Royal Veterinary and Agricultural University, DK-1958 Frederiksberg C, Denmark*
[c] *Aalborg University, Esbjerg (AUE), Niels Bohrs vej 8, DK-6700 Esbjerg, Denmark*

Received 1 June 2001; accepted 12 February 2003

Abstract

This paper gives an overview of multi-way methods in image analysis, termed *N*-way image analysis. Both weak and strong multi-way methods are applied in order to decompose and characterize image data, and obtain insight into their abilities to capture and model the interpretable data structure. Multivariate Image Analysis (MIA) is a typical example based on weak multi-way methods like *unfold*-PCA/PLS. Strong multi-way methods such as PARAFAC, Tucker3, N-PLS are also introduced and applied to image analysis in this work. Which method to use is problem-dependent. Through macroscopic satellite images, virtual fluorescence images and microscopic functional property image examples, the performance of each alternative method is presented, as well as comparisons between weak and strong multi-way models. It is demonstrated that efficient handling of multiple images requires a clear a priori overview of the relationship between problem formulation and data array configuration. Appropriate preprocessing techniques, such as 2-D FFT and Wavelet transform, may also be needed in order to transform and configure some special types of image data to forms specifically suited for multi-way modeling. Application I shows the possibility for application of strong multi-way methods on multispectral images, otherwise conventionally analyzed by MIA. By contrast, application II attempts to investigate the feasibility of applying MIA models on typical three-way data, normally handled by the strong multi-way methods and provides a new perspective of dealing with fluorescence spectra as images. In application III, attempts have been made to predict rheological parameters from microscopic cheese images by multi-way methods. The present *didactic* exposition allows to draw some tentative first conclusions as to the dominant relationships between strong and weak multi-way data decompositions, their pros and cons and their relative merits.

Keywords: Multivariate Image Analysis (MIA); Multi-way methods; Unfolding; Image; PCA/PLS; PARAFAC; Tucker3; N-PLS; 2-D FFT

1. Introduction

Many chemometric methods have been employed in dealing with more complex images, especially in spectroscopic imaging [1–10]. In this work, attempts

* Corresponding author. Tel.: +1-203-402-5303; fax: +1-203-944-4925.
E-mail address: Jun.Huang@perkinelmer.com (J. Huang).

0169-7439/03/$ - see front matter © 2003 Elsevier Science B.V. All rights reserved.
doi:10.1016/S0169-7439(03)00030-3

have been made to apply multi-way methods to image analysis, defined as *N*-way image analysis. It handles *multiple* images simultaneously using information from different dimensions as opposed to just of *one single* image. In multispectral imaging, for instance, both spatial and spectral information could be used to extract information.

Multivariate Image Analysis (MIA) is one particular approach to *N*-way image analysis. Principles and applications of MIA have been developed in full detail in the past decade. Typical examples are related to multispectral images such as satellite images, microscopic images, etc. [1–10]. Below we have tried to apply strong multi-way methods on multispectral images which are otherwise conventionally analyzed by the MIA approach as well as to apply MIA on three-way (fluorescence) data usually handled by strong multi-way methods. Another focus of this work is concerned with serial images that are more easily obtainable than multispectral images, which possess certain common properties and interrelationships. Thus microscopic cheese images, to be introduced in application III, were made from a factorial experiment by varying coagulation temperature and the amount of rennet enzyme at a number of levels. They are of quite similar appearance and also possess similar rheological characteristics, but they do not fit any of the two above conventional three-way array formats. They can nevertheless be juxtaposed, by transforming and reorganizing them so as also to comply with the form of a three-way data array suitable for multivariate data modeling. Attempts have been made to derive functional properties prediction models to predict the rheological properties from images by *N*-way image analysis.

The objective of this survey is to review the gamut of multi-way methods from the perspective of *proper* (i.e. problem-dependent) data array organization and the many multi-way methodological methods presented in the literature. Within three-way/multivariate image analysis, there has been a rather bewildering ad hoc modus operandi concerning how to organize the pertinent object-way(s), variable way(s), time way, etc., and what particular method to use. We here focus on the systematic correspondence between the specific multi-way problem formulation and their *matching* data array setups, from which follows which methods are at all possible—or not. We want to show that exploitation of multi-way methods is not a free optional matter, but rather that it is in many ways more logically restricted by the problem/data array prerequisites. Therefore, our survey is also composed of ‘‘cross-over’’ methodological experiments in order to present a fairly complete catalogue of representative usages of the many multi-way methods.

2. Terminology and nomenclature in *N*-way image analysis

2.1. Terminology

Some confusion and misunderstandings may arise when dealing with multivariate analysis on images and other types of *N*-way arrays. It is therefore necessary to give a clear explanation of the terminology and nomenclature to be used in the following. An intensity/gray-level image can be 2-D, 3-D or N-D. The images discussed in the present context are in 2-D form. The term *N*-way image analysis is characterized by multivariate analysis of a stack of images in general. *N*-way image data consist of a stack of images which usually have similar properties, i.e. chemical, biological characteristics or inherent correlations, or intrinsic variations, etc. A multivariate image is a stack of *congruent images* on the same field-of-view measured for a series of different ‘variables’, e.g. wavelength, frequency, etc. [3]. Multi-way methods can be categorized into weak and strong multi-way methods [11]. Unfold-PCA/PLS are considered weak multi-way methods because they actually unfold three-way data array into two-way, followed by ordinary two-way analysis, instead of utilizing the intact multi-way structure during the modeling. It should be noted that the term multi-way PCA (MPCA) has been used in chemometrics for unfolding and doing ordinary PCA (hence Tucker1) modeling. Bro pointed out that it is improper to use this term since it is easily confused with multi-mode PCA, which is the term accepted for the Tucker models in general [10,11]. Thus, we use here the term unfold-PCA/PLS instead of multi-way PCA/PLS to avoid further confusion. Strong multi-way methods usually refer to the trilinear PARAFAC model, Tucker3 model, and the more advanced PARAFAC2 and PARATUCK models, which distinguish them-

selves from unfold-PCA by explicitly using the multi-mode structure in the data in general, and they also offer different attractive features. Multilinear calibration is a strong multi-way regression approach, together with which PARAFAC and Tucker3 models will be used in our first forays at *N*-way image analysis below.

2.2. Nomenclature

In the following, digitized images are denoted by bold capitals, and three-way (image) array by underlined bold capitals. Lower-case italics are used for scalars, and bold lower-case characters for vectors. The letters, *I*, *J* and *K* are reserved for indicating the dimension of different modes. The *ijk*th element of $\underline{\mathbf{X}}$ is called x_{ijk} and is the element in the *i*th row, *j*th column and *k*th tube of $\underline{\mathbf{X}}$. The name *way* is defined as geometrical dimension, and the name *order* indicates number of ways. Object modes are denoted by bold capital letter **O**, and variable modes by **V,** following Esbensen et al. [2].

3. Data configuration in multivariate data analysis on images

3.1. Data array categorization in N-way image analysis

Choosing an optimal data analytical methodology requires an appropriate data configuration pertaining to specific problem formulations in multivariate data analysis. *N*-way image analysis is no exception. The proper arrangement of a large amount of image data is intimately connected with the scientific goal or the pertinent problem formulation. A matrix, in ordinary two-way analysis, is conventionally arranged in a way such that the rows of a matrix represent samples (observations), and the column variables. We use **O** to represent samples (observations), viz. the *object mode*, and **V** the *variable* mode. Arrays of three-way data thus can be characterized by a categorical object/variable (**O**/**V**) mode convention, which was introduced in Refs. [9,14]. The entire class of all possible four different three-way configurations are represented by the codes (**OOO**), (**OOV**), (**OVV**) and (**VVV**), of which the last extreme is usually of lesser practical consequence for multivariate data analysis; we do however treat the **OOO** case extensively below. A three-way data array composed as a multivariate image, for instance, may be characterized as **OOV**, while the well archetype three-way data array corresponds to the **OVV** form.

The **O**/**V** definition may serve as a guide to properly arrange the complex data arrays of higher-order and choose the appropriate preprocessing and multi-way methods. In two-way analysis, conventionally, centering is usually performed across the object mode (the rows of a matrix), while scaling is performed within the variable mode (the columns of a matrix). Centering across the object mode means that the data are centered by subtracting the column-average from every element in the column. When scaling within the variable mode, every column is multiplied by a specific number, e.g. 1/STD. Preprocessing of a higher-order array is more complicated than in two-way analysis. Centering is normally performed across the object mode(s). Given an **OVV** array of $\mathbf{I} \times \mathbf{J} \times \mathbf{K}$ matrix with **I** representing object mode, centering can be done by unfolding the array to an $\mathbf{I} \times \mathbf{JK}$ matrix, and then center this matrix as in ordinary two-way analysis:

$$X_{ijk}^{\text{cent}} = X_{ijk} - \sum_{i=1}^{I} X_{ijk} \Big/ \mathbf{I}$$

Centering, however, is different when it applies to an **OOV** array of $\mathbf{I} \times \mathbf{J} \times \mathbf{K}$ matrix with **I**, **J** as object modes. The **OOV** array is unfolded to an $\mathbf{IJ} \times \mathbf{K}$ matrix and then center this matrix. It is not, as for scaling, appropriate to scale the unfolded array column-wise, but rather whole slabs or sub-matrices of the array should be scaled within variable modes. For a complete delineation of centering and scaling, see Bro and Smilde [20].

3.2. Data analytical problem formulations

A significant part of multivariate data analysis can be covered by the following three alternative objectives/problem formulations:

(1) data description (exploratory data analysis);
(2) classification and discrimination;
(3) correlation and regression.

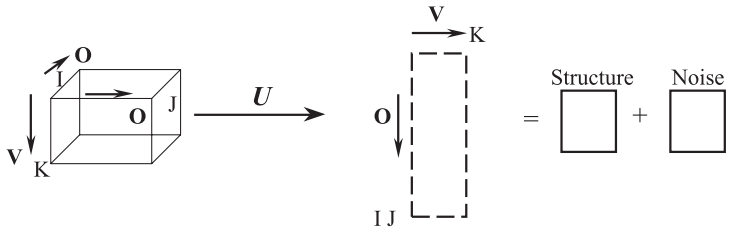

Fig. 1. A three-way array is unfolded to a two-way array, on which the PCA is then performed. ***U*** denotes the *unfolding* operator.

This partitioning is not complete, but can serve as a systematic basis also for carrying out higher-order data analysis, see more detail in [Ref. 2].

3.3. Relationship between data configuration and problem formulation in three-way image analysis

Major types of data modeling in *N*-way image analysis are described in the following with focus on the **OOV** and **OVV** data arrays.

3.3.1. Data description

A multivariate image is a two-way array (**OO**) with a third way as the variable mode (**OOV**). The standard MIA way of doing multivariate image analysis is to reorganize/unfold the three-way data array to two-way first, and then to perform ordinary two-way analysis on unfolded 2D array. The approach is usually termed unfold-PCA/PLS if used in conjunction with PCA/PLS. Due to its original three-way arrangement and inherent unfolding, unfold-PCA/PLS can be categorized as a weak multi-way method. See the graphical presentation in Fig. 1.

For an image array with **OOO** structure, domain transformations may occasionally be implemented to obtain an **OVV** or **OOV** array which is trilinear and thus suited for strong multi-way analysis. We give one such example in application III later (Fig. 2).

3.3.2. Classification and discrimination

One of most important demands on image analysis is to extract information pertaining to classification or discrimination of pixels in one or more classes, or of one or more entire images, depending on the specific problem to be solved. There are two principal types of classifications in terms of **OOV** and **OVV** data array configurations. For **OOV** data array, classification is performed simultaneously within **OO** planes. For **OVV** data array, however, classification is performed along the object mode. One single plane here represents one object only.

3.3.3. Regression

When regression modeling is applied to three-way image data, it is called three-way image regression. There are three basic types of regression in three-way image regression. Image regression can be established not only between images, but also between image data and physical or chemical properties of what has been imaged. The latter will be focused in application III, which is concerned with regression between microscopic images and rheological properties of cheeses. Multivariate Image Regression (MIR) based on unfold-PLS has recently been reformulated with details to be found in Lied et al. [10]. MIR deals with **OOV** data arrays exclusively.

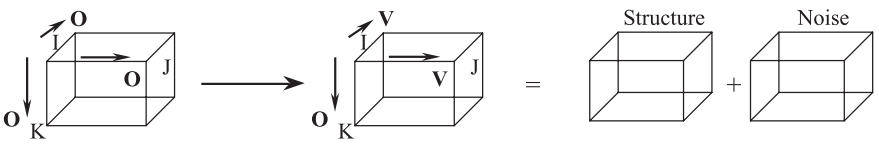

Fig. 2. An **OOO** three-way data array has to be transformed to an **OVV** (or the **OOV** alternative) data array, which is suited for subsequent multi-way modeling.

4. Theory on multi-way decomposition methods

4.1. Weak multi-way methods

As discussed in Section 3, unfold-PCA/PLS is categorized into the family of weak multi-way methods. Unfolding the higher-order arrays may break the correlations in either (**OO**) or (**VV**) modes.

4.1.1. OOV three-way image data array

The typical **OOV** three-way image data array consists of **K** images of size $\mathbf{I} \times \mathbf{J}$ measured, e.g. at **K** wavelengths. The three-way matrix $\underline{\mathbf{X}}$ ($\mathbf{I} \times \mathbf{J} \times \mathbf{K}$) is *unfolded* into a two-way array so that each image pixel works as an object while each wavelength (or frequency, energy, etc.) is maintained as a variable. Then PCA is performed on the two-way data set ($\mathbf{IJ} \times \mathbf{K}$). With unfold-PCA, in each component the data are decomposed into a long score vector (**IJ**) which can be rearranged to a two-way score image ($\mathbf{I} \times \mathbf{J}$). The loading vectors $\mathbf{p}_f$ ($\mathbf{K} \times 1$) describe the variations in variable space for each component. The model can be written

$$\underline{\mathbf{X}} = \sum_{f=1}^{F} T_f \mathbf{p}_f + \underline{\mathbf{E}}$$

The index f denotes a component, and $\underline{\mathbf{E}}$ residual images from unfold-PCA. The components are orthogonal and can be calculated sequentially.

4.1.2. OVV three-way image data array

Decomposition of the **OVV** three-way image array is different from **OOV**. The distinction is that unfolding is now performed on the two-way variable mode instead of object mode. As compared to **OOV** (e.g. MIA) data decomposition, the three-way **OVV** array matrix $\underline{\mathbf{X}}$ ($\mathbf{I} \times \mathbf{J} \times \mathbf{K}$) is *unfolded* into a two-way array ($\mathbf{I} \times \mathbf{JK}$) where the object direction of the images is maintained intact (the sample mode). Likewise, in each component the data are decomposed into a score vector ($\mathbf{I} \times \mathbf{1}$) in sample image mode, $\mathbf{t}_f$, and a long loading vector (**JK**) which can subsequently be *backfolded* to a two-way loading matrix $\mathbf{P}_f$ ($\mathbf{J} \times \mathbf{K}$) (or loading image). $\mathbf{P}_f$ describes the variation in the 2-D variable domain space for each component. The structure model with residuals is

$$\underline{\mathbf{X}} = \sum_{f=1}^{F} \mathbf{t}_f \mathbf{P}_f + \underline{\mathbf{E}}$$

4.2. Strong multi-way methods in N-way image analysis

Some strong multi-way methods such as PARAFAC and Tucker3 can be adapted to image analysis. PARAFAC is a direct trilinear decomposition method, conceptually comparable to bilinear PCA, while the Tucker3 decomposition is another generalization of PCA to higher orders [12,13,16,17]. A detailed tutorial on PARAFAC is given by Bro [13]. A PARAFAC model of a three-way array is expressed by *three-loading matrices*, **A**, **B** and **C** with elements a_{if}, b_{jf}, c_{kf}, and the residuals. It can be written

$$x_{ijk} = \sum_{f=1}^{\mathbf{F}} a_{ij} b_{jf} c_{kf} + e_{ijk}$$

where **F** is the number of components, e_{ijk} denotes the residual elements.

Both PARAFAC and Tucker3 are simpler than the alternative approach, unfold-PCA, due to fewer parameters in the models. A Tucker3 model is a weighted sum of all possible outer products between the factors stored as columns in **A**, **B** and **C** with the weight of the outer products determined by a core array $\underline{\mathbf{G}}$ ($\boldsymbol{w}_1$, $\boldsymbol{w}_2$, $\boldsymbol{w}_3$). It can be written in a same manner to PARAFAC

$$x_{ijk} = \sum_{d=1}^{\mathbf{D}} \sum_{e=1}^{\mathbf{E}} \sum_{f=1}^{\mathbf{F}} a_{id} b_{je} c_{kf} g_{\mathrm{def}} + e_{ijk}$$

where the index **D**, **E**, **F** denotes the number of components in each mode, and g_{def} the elements of the core array $\underline{\mathbf{G}}$.

4.3. Multi-way calibration

There are many possible multi-way calibration methods, among which unfold-PLS and N-PLS associated with a trilinear (PARAFAC-like) model are introduced here. Unfold-PLS is characterized by per-

forming ordinary PLS on a two-way array unfolded from a three-way array and **y** variable(s), while keeping the object mode of $\underline{\mathbf{X}}$ in common with the dependent **y** intact, see e.g. Lied et al. [10].

Details on multilinear calibration are given by Bro [14] and Smilde [15]. Bro pointed out that the advantages of N-PLS (including tri-PLS) over unfold-PLS can be highlighted by the following two points: (1) the trilinear model is more parsimonious, simpler and thus easier to interpret; and (2) less prone to noise due to decomposition across all modes [12]. However, there is no general rule in choosing which method to use. The knowledge of data sets under investigation and a priori knowledge of calibration methods, proper problem formulation, is always an important guideline. For instance, we have often found that unfold-PLS works very well in multivariate image regression (MIR) [10], by virtue of inherent weak correlations *between* the singular variable way and the two object ways, which internally of course display strong, contextural correlations, etc. Conversely, there *may* a priori exist *possibilities* for applying N-PLS in multivariate image regression, i.e. finding regions of interest.

In the following sections, three application examples on multispectral images, virtual fluorescence images and microscopic image-functional property correlation using above methods will be given.

Both weak and strong multi-way methods are applied in order to decompose and characterize image data, and obtain some insight into their abilities to capture data structure. Applications I and II use both MIA and strong multi-way methods on typically MIA data and strong three-way data in order to evaluate their scientific playgrounds. Application III in addition attempts to investigate the relationships between transformations of original images and their corresponding functional properties. Comparisons of the

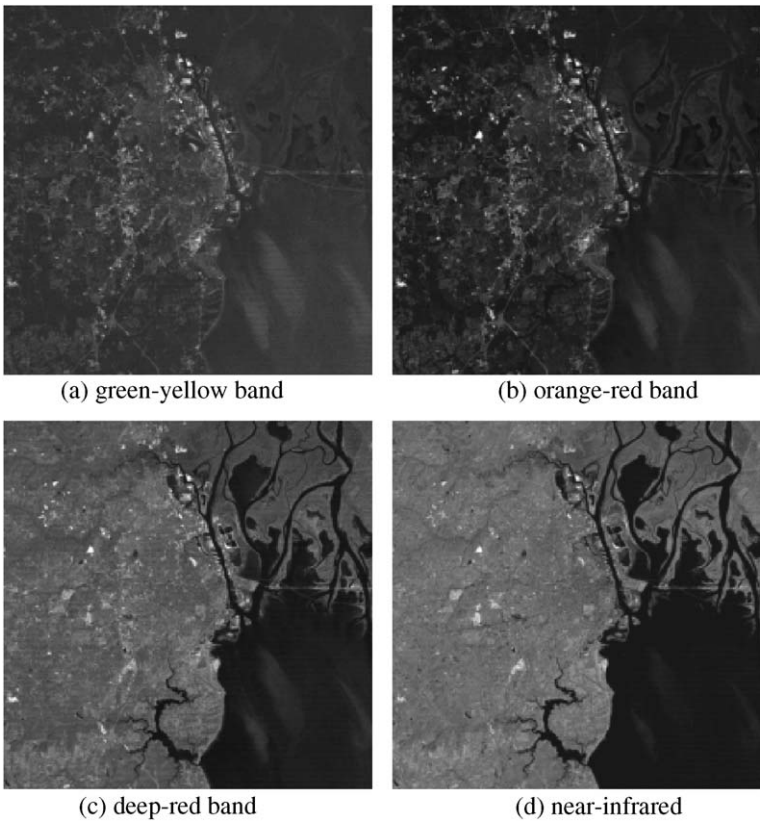

Fig. 3. The 512 × 512 satellite image recorded at four different wavelength bands.

ability of these methods are given. The goal of comparison is not to verify one method over another, but rather to explore alternative approaches to *N*-way image analysis.

5. Application I: Multi-way analysis of OOV image array (multispectral image example)

5.1. Data

This data set, Fig. 3, is a multispectral satellite image of Mobile Bay, Alabama, which has been described in the chemometric literature (Geladi and Esbensen). It is made up of four variables (''channels''), the wavelength bands. In each wavelength band, the reflected intensities of the earth surface are digitized in the range 0–127. One pixel is about 80 × 80 m.

This is a typical **OOV** image array (512 pixels × 512 pixels × 4 wavelengths) where the two spatial directions form the object modes and the wavelengths form a variable mode. In the following, both weak (unfold-PCA/Tucker1) and strong methods (PARAFAC and Tucker3) are applied to this **OOV** image array. Mean-centering was performed across the object mode (pixels). Scaling by standard deviation was carried out within the variable mode (wavelength bands).

5.2. Multi-way analysis of multispectral images

5.2.1. Unfold-PCA model (Tucker1 model)

This type of multispectral image is an archetype for MIA. MIA's objective is to conduct unfold-PCA

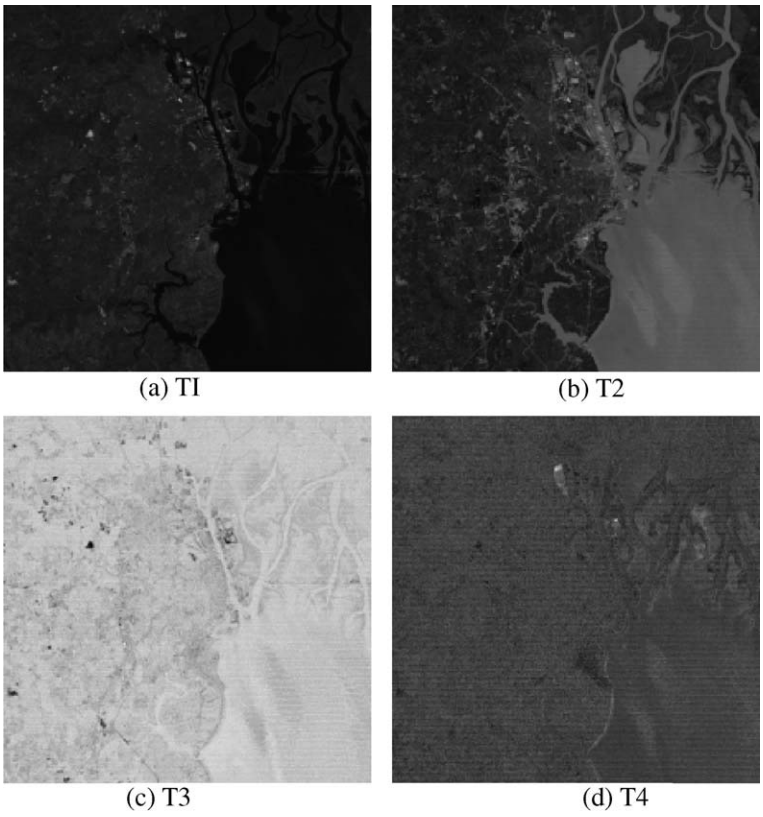

Fig. 4. The four score images of the 4 × 512 × 512 satellite image: T1, T2, T3, T4. The first three contain most information, while the last image contains very nearly only residual noise and artifacts. The score images are in maximum contrast with each other as a result of the inherent MIA orthogonality of the scores.

analysis on the multivariate image, i.e. to conduct an interactive study of scene (raw images/score images) and feature space (score and loading plots). The score images are obtained after the PCA calculations on these four raw images (four variables). Score images are in maximum contrast to each other due to orthogonality of the PC scores (Fig. 4). Residual images are not shown here, which contain mostly the noise largely from electro-optic instrument artifacts, already appearing in T4.

5.2.2. PARAFAC model

A three-component PARAFAC model is now fitted to the same image array for direct comparison. Fig. 5 shows a set of four reconstructed images from the structure model in the order of number of components. The reconstructed image has the same size as raw image array. Notice the extreme difference with respect to Fig. 4. These four images appear extremely blurred (but the profiles of bay in images (b), (c), (d) are perhaps faintly discernable). It is apparent that PARAFAC failed in modeling the multivariate image variance efficiently in this case. The reason is that three components are not enough to account for the most variation as PARAFAC modeling requires equal components in all modes. There are only 4 wavelengths in variable mode, and as many as 512 pixels in two object modes. Few variables make it impossible to choose enough components for a well-fitted model. As clearly seen from modeling results, three components are not capable of explaining major variations along three modes.

5.2.3. Tucker3 model

A Tucker3 model offers more flexibility than PARAFAC in that it allows for a choice of different number

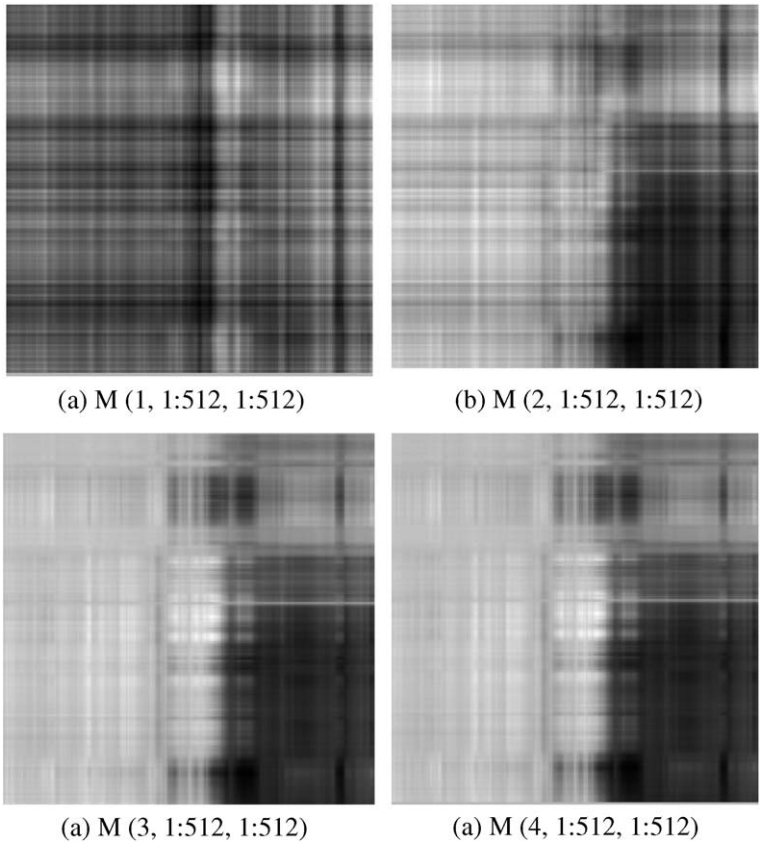

Fig. 5. Reconstructed structure parts from a three-component PARAFAC model. Notice the extreme difference with respect to Fig. 4.

of components in the different modes. Therefore, we can choose more components precisely in the two object modes unlike for the PARAFAC model. Different component options have been tried out. After trial and error, 3 components are chosen in the variable mode, and 64 components in each object mode, as this model captures 98.93% of the total variance. The reconstructed images from structure part are shown in Fig. 6. This structural model is calculated from $\underline{\mathbf{X}\ \text{structure}} = \mathbf{AG}\ (\mathbf{C}^{\mathrm{T}} \otimes \mathbf{B}^{\mathrm{T}})$, where **A**, **B**, **C** are loading arrays, and **G** core array, and the symbol $\otimes$ denotes Kronecker multiplication, see [Refs.16,17].

In the order of number of components, the reconstructed images (by proper image analysis scaling in the structural model) appear quite clear and optimally contrasted. They are complementary to each other, but it should be noted that reconstructed images here are not exactly orthogonal to each other, which is different from score images derived from unfold-PCA model. Clearly, a Tucker3 modeling provides a different approach to describe the image data from a new perspective. Tucker3 modeling of multispectral images may be useful for, e.g. de-noising, data compression, visualization, etc. Residual images are not

Table 1
Cumulative variations captured by unfold-PCA, Tucker3 and PARAFAC models

Number of components/ factors	Unfold-PCA (%)	Tucker3 (%)	PARAFAC (%)
1	86.55	91.41 (1, 64, 64)	89.57
2	99.13	97.86 (2, 64, 64)	94.28
3	99.66	98.93 (3, 64, 64)	94.76

For Tucker3 model, 64 components are chosen in each object direction, while the components in the variable mode vary from 1 to 3.

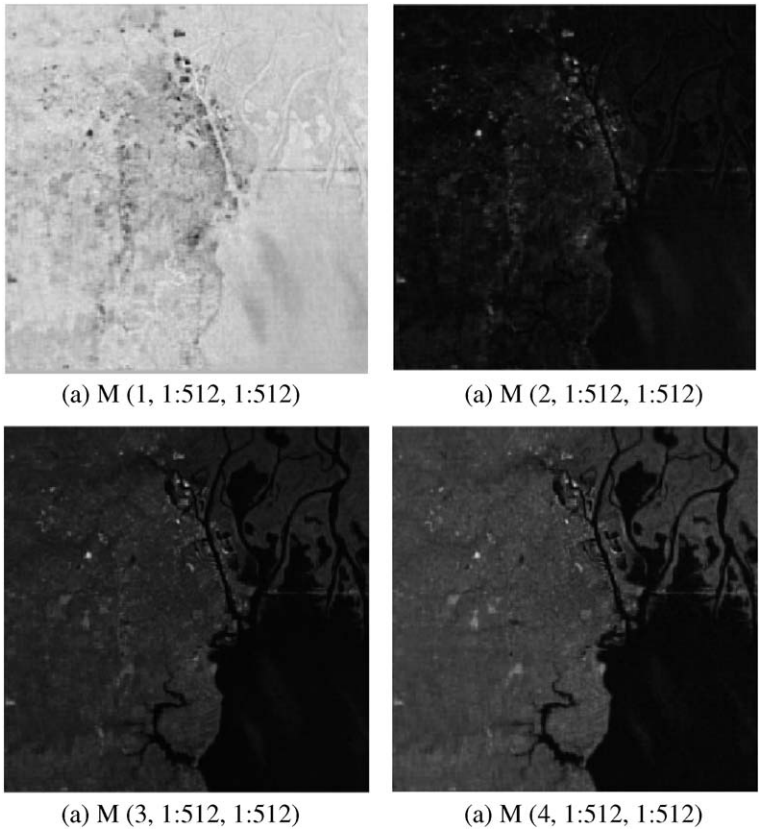

Fig. 6. Reconstructed structure parts from a Tucker3 model with (3, 64, 64) components in each of the three mode (**VOO**). Notice the differences with respect to Fig. 4.

shown here. They are mostly random noise due to possible illumination, nonlinear optical behavior, etc. The Tucker3 model successfully captures most of the image variance with this (3, 64, 64) setup of components.

It is interesting to compare these three different methods on this type of OOV image data array. Table 1 gives the percentage of variations explained after 1, 2, 3 components (in first mode for Tucker3). With three components, unfold-PCA explains the largest variation, 99.66%, followed by Tucker3, 98.93% and PARAFAC, 94.76%. This is understandable since PARAFAC is most parsimonious. Furthermore, both unfold-PCA and strong three-way models

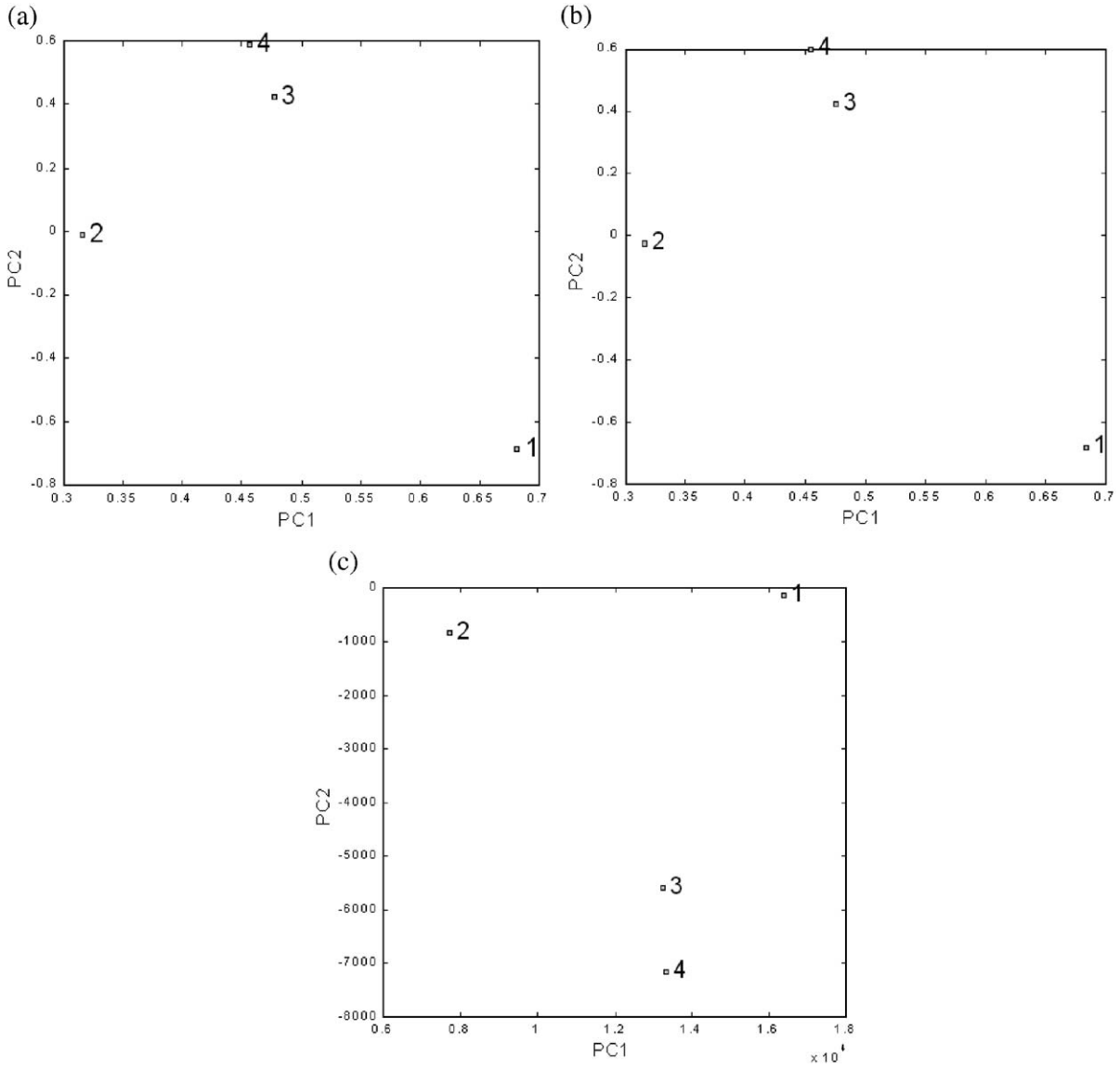

Fig. 7. Loading plots (**p**1 vs. **p**2) in the variable mode from different models. (a) Unfold-PCA/Tucker1 model; (b) Tucker3 model; (c) PARAFAC model.

maximize the fit of model to the data in the bilinear and trilinear sense respectively. It is not difficult to see that unfold-PCA is just Tucker1 in the specific sense that the model is fitted. Therefore, MIA and other three-way/*N*-way modeling of images form different cases of *N*-way image analysis. In the above unfold-PCA/Tucker1 model, two object modes are left uncompressed, and only the variable mode is compressed. The object modes and variable mode are compressed with different number of components in Tucker3 model, whereas the PARAFAC model compresses all modes with an equal number of components. It is also of interest to compare the respective loading plots from the three models as shown in Fig. 7. Loadings from the unfold-PCA and Tucker3 models show very small differences only, but differ somewhat from the PARAFAC model. The reason is that the Tucker model compresses three modes separately, and establish a relationship between factors in the three modes spanned by the core array. Here both Tucker1 and Tucker3 use 3 factors in the variable mode. As compared to Tucker models, PARAFAC does not have a core array to allow this flexibility in choosing different factors. The three factors here are directly interrelated to each other. However, on the general level all three models show almost the same interrelationships in this particular example.

Which model to use is problem dependent. The MIA approach is based on unfold-PCA, for instance, which offers the tools for data decomposition and interactive study of scene and feature space for segmentation and classification, etc. The latter is largely due to the fact that pixels in two-object modes are kept uncompressed, and thus pixels in the score plot correspond to those in score images backfolded from scores after unfold-PCA. Therefore, MIA is probably better suited for explorative data analysis and classification purpose, etc., while the Tucker3 model could be used for image data compression, exploration of three-way structure, de-noising, etc. The PARAFAC model may only be considered when there are approximately as many variables as comparable to objects present.

A significant amount of practical work still needs to be done in this area before a more satisfactory body of experience is at hand.

6. Application II: Decomposition of fluorescence data with MIA (virtual spectroscopic image example)

6.1. Data set

This data set was obtained from Rasmus Bro, KVL, Copenhagen. It has analogously to the Mobile Bay data array been used in many three-way data decomposition expositions. Five samples were measured on a PE LS50B spectrofluorometer with excitation 250–300 nm, emission 250–450 nm in 1-nm intervals. Two samples contain different amounts of tyrosine, tryptophane and phenylalanine [13] (see Fig. 8a and b). Three other samples are pure components of these three analytes, respectively (see Fig. 9a–c). This is an archetype trilinear three-way data (OVV). It has been demonstrated that the three pure spectra can be estimated almost perfectly by the unique PARAFAC decomposition of the fluorescence spectra of two samples containing different amounts of Try, Trp, and Phe, see details in [Ref. 13].

In the present context, it is not our intention to seriously pit the MIA approach against the strong three-way methods (PARAFAC), but rather to analyze such spectroscopic data from an imaging point of view only—in order to investigate the possibilities and limitations of applying MIA on three-way (**OVV**) spectroscopic data. The reason is that virtually every spectroscopic technique can be used to generate chemical images. Fluorescence data is a very good example of this since each sample is a ‘‘landscape’’ composed of the excitation and emission spectra. Intuitively, such a landscape may well also be considered as an image with appropriate conversion/scaling (see Figs. 8c,d and 9d–f).

6.2. Results and discussion

Fluorescence spectra of the two samples with a mixture of three analytes were first converted into appropriately scaled images, and then put into a MIA model. Auto-scaling was applied to data. The score image (printed in grayscale) shown in Fig. 10 is in reality a pseudo-color composite formed by assigning score image 1, 2, 2 into R, G, B channel for a visualization purpose. As seen in Fig. 10, the three analytes can be seen clearly with different colors (shown by

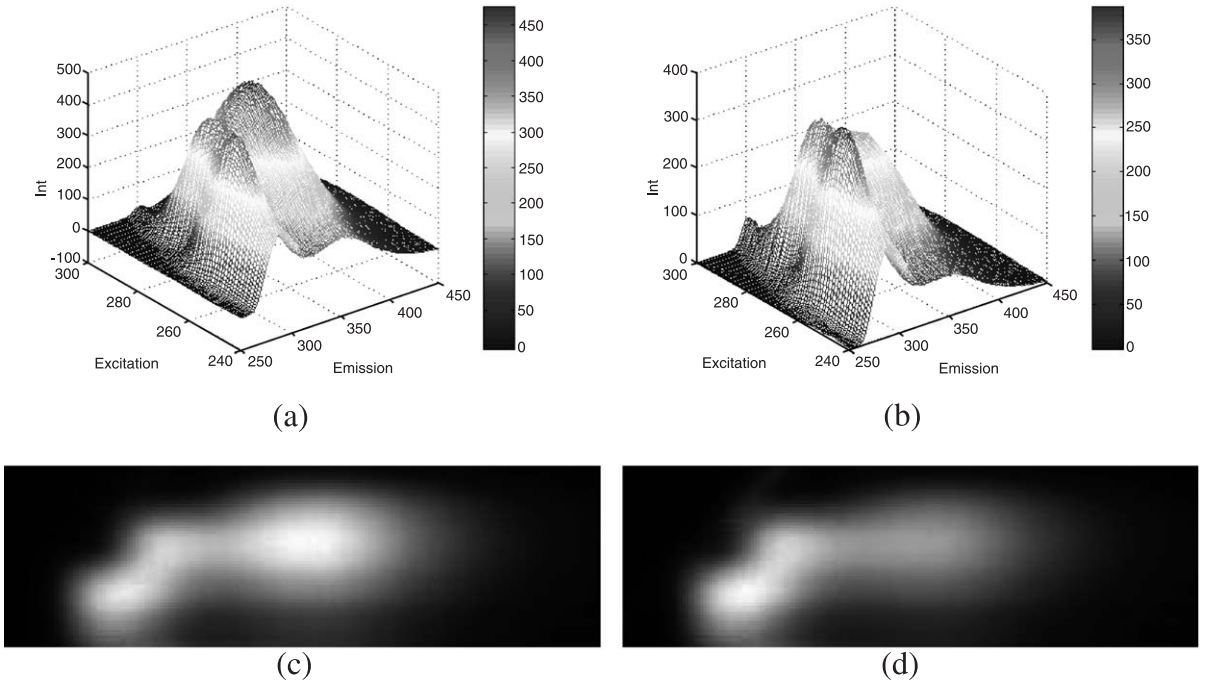

Fig. 8. (a) Fluorescence spectra of a sample containing different amounts of Trp, Tyr and Phe. (b) Fluorescence spectra of another sample containing different amounts of Trp, Tyr and Phe. (c) Image converted from the spectra corresponding to (a). (d) Image converted from the spectra corresponding to (b).

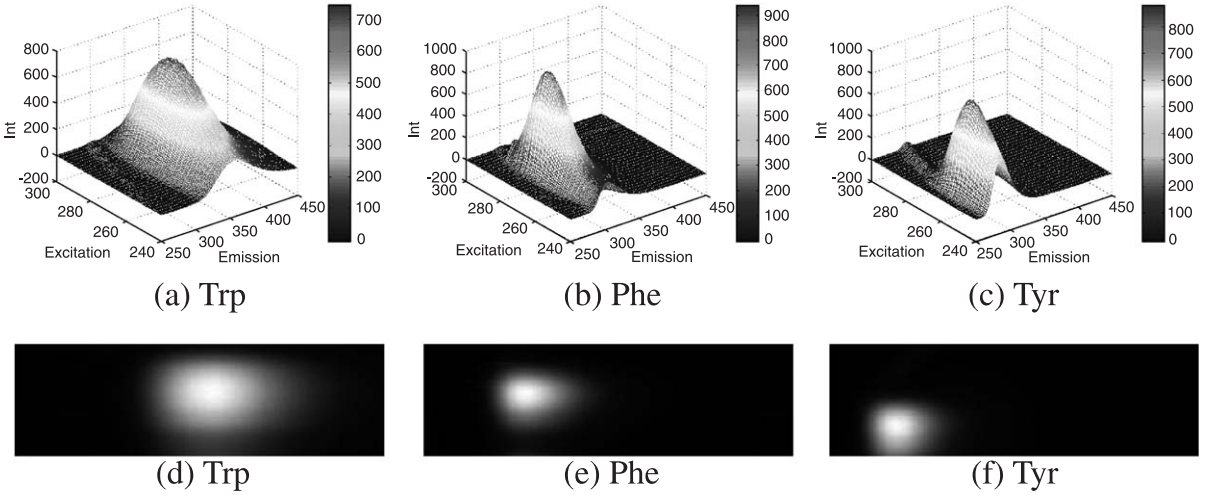

Fig. 9. (a) The pure fluorescence spectra of a sample containing only Trp. (b) Pure fluorescence spectra of a sample containing only Phe. (c) Pure fluorescence spectra of a sample containing only Tyr. (d) Converted image representing Trp. (e) Converted image representing Phe. (f) Converted image representing Tyr.

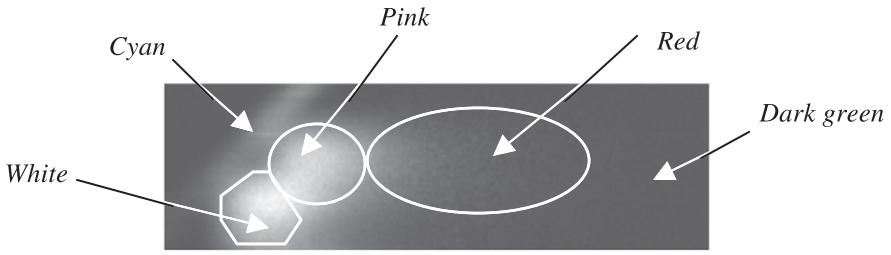

Fig. 10. Pseudo-color composite (printed in grayscale) obtained by assigning score image 1, 2, 2 into R, G, B channel. Note the regions of interest are represented by different colors: Red (Trp); Pink (Phe); White (Tyr). Cyan (Rayleigh scatter).

approximately enclosing markings). Notice the *Rayleigh scatter* (the triangular part in the upper left corner), which is easily distinguished in the image. This is, however, very obscure in the original images shown in Fig. 8. The shape of each analyte is similar to the corresponding pure component image in Fig. 9d–f.

An interactive study of score plots (feature space) and score image (scene space) is conducted in a conventional MIA fashion shown in Figs. 11 and 12. Four groups, which correspond to three analytes and the *Rayleigh scatter* effect, respectively, can be classified easily by mapping typical MIA masks in score plots (**t**1–**t**2). These selected areas are then projected so as to be compared to the corresponding chemical analytes in scene space (score image, Fig. 10). See details about this feature of MIA operations in [Refs.3–9].

As is easily seen, MIA does not provide precise results quantitatively as compared to the PARAFAC model, and neither is MIA aimed at such an objective. However, it does offer a simple way of direct visualization of spectroscopic/image data which may be useful in more complex situations, e.g. forensic analysis, etc. It may be helpful to look at the data visually and study the spatial chemical data interactively in appropriate situations.

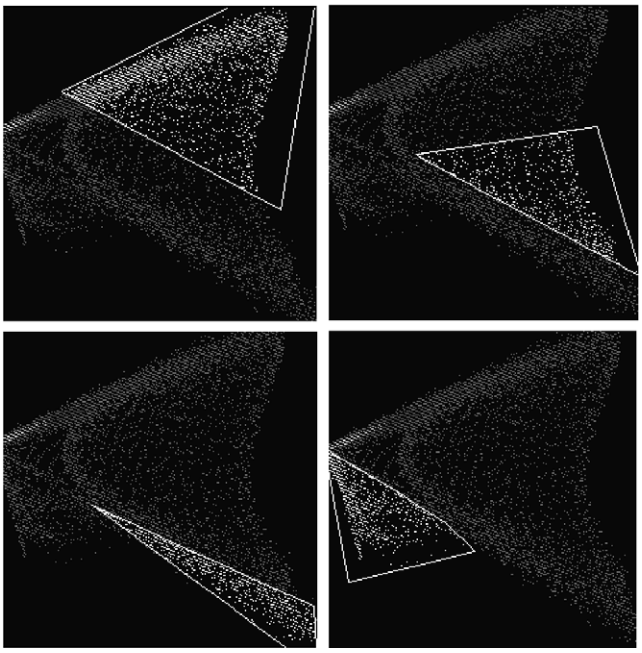

Fig. 11. Score plots (**t**1–**t**2) by plotting two score images against each other. Clusters indicated by different polygonal MIA *masks* represent different groups in the image plane, see Fig. 12.

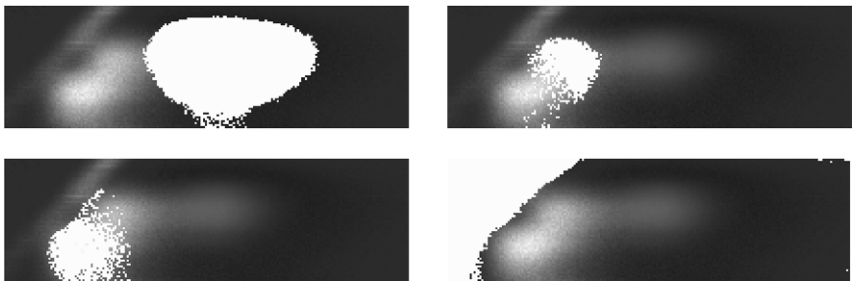

Fig. 12. Regions of interest here marked in white color in the image plane originate from the corresponding pixel masks delineated in the score plots in Fig. 11.

In conclusion, applying a MIA model on the fluorescence three-way data (**OVV**) of course does not seem to be a natural idea for the purpose of quantitative decomposition of the data. The reason is that the MIA approach is specially designed for **OOV** multivariate image data. However, our objective here only is to propose imaging as a *complementary* way of ''qualitative spectroscopy'', which may change one's perspective to recognize some spectroscopic problems in a possibly fruitful new light.

7. Application III: Multi-way analysis of OVV image arrays (microscopic image example)

7.1. Data set and problem formulation—"incongruent multiple images"

Images in many areas such as biochemistry have largely been analyzed by traditional image analysis. These methods tend to be restricted for use in one single image at a time. There is a lack of good methods which can be used to characterize series of images efficiently. With multivariate data analysis on images, many serial images can potentially be analyzed simultaneously.

Fourteen types of cheeses were made from a factorial experiment where coagulation temperature with rennet enzyme, the amount of rennet enzyme and the length of time at coagulation temperature before cooling were varied, i.e. a three-factor experiment. For each of these cheeses, four transmission electron micrographs were recorded on four different parts of the cheeses. Each set of four images therefore constitutes four replicates of the same cheese. As seen from selected images shown in Fig. 13, such cheese images appear relatively homogenous and very similar at first glance. The objective is to relate these global images to selected functional properties to the cheeses by *N*-way image analysis.

Uniaxial compression, a rheological testing method, has been used to obtain the rheological properties of these cheeses, such as fracture stress, strain, work and modulus. From a biotechnological point of view, it would obviously be of interest to look for the relations between the 'image' results and the 'rheological' results. Therefore, unfold-PLS and N-PLS are used to achieve this goal below and to be compared.

7.1.1. Necessary transformations

As inspected from the raw cheese images in Fig. 13, at a certain scale they appear relatively homogeneous and quite ''similar''. This is manifestly *not* a multivariate image, not even a congruent image field-of-view, but a series of one-channel images for which there does not exist any preexisting *N*-way method. There is currently a lack of efficient methods to characterize and discriminate such multiple images in traditional image analysis. Some image analysis combined with chemometric methods have been initiated on this problem especially concerning the interesting new AMT-transformation, but this is deferred to a later occasion [18,19]. Here we focus on the familiar 2-D FFT transformation.

The 14×4 serial images of size 512×512 are stacked on top of each other to form a three-way array, which will be of the **OOO** category. This type of data array is obviously not trilinear, and thus cannot be used for multi-way analysis directly. Different trans-

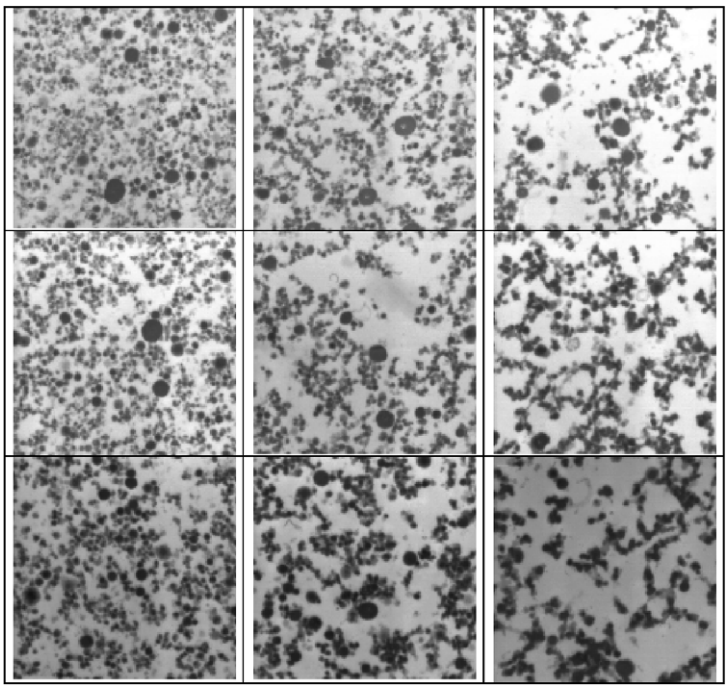

Fig. 13. Microscopic images of cheeses (1–9), originating from a factorial experiment by varying coagulation temperature and the amount of rennet enzyme, each on three levels. Note the quite similar appearance.

formation techniques such as FFT, Wavelet Transform (WT), have been applied to this **OOO** data array in order to obtain a trilinear **OVV** data array. Such a transform is necessary to bridge the gap between each image through the new domain. FFT-transformed data (power spectra) are used for illustration here since these give the most illustrative models (see Fig. 14).

As appreciated, these 64 images of size 512 × 512 comprise a large amount of data, and will cause a long calculation time when applying three-way methods. All 64 images were therefore resized to 64 × 128 × 128 and transformed to 2-D FFT array of size 64 × 128 × 128 so that the time spent on actual modeling could be decreased significantly. All modeling was carried out with *the N-way toolbox for Matlab* by Andersson and Bro [16,17]. Image processing and transform were conducted with the signal processing and image processing toolbox in Matlab 5.3.

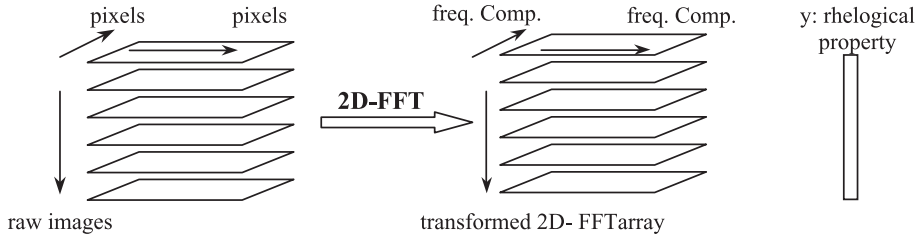

Fig. 14. Data configuration of cheese image data for subsequent modeling. Raw images are organized as a three-way **OOO** data array, and subsequently transformed by 2-D FFT to a three-way **OVV** array, in which the 2-D frequency domain forms the two new variable modes (**VV**). Vector **y** represents a rheological property which corresponds to the individual original images in the **O**-direction.

7.2. Prediction of rheological properties of cheeses

For each cheese, a rheological testing was applied independently, and thus the rheological properties are known, e.g. fracture stress, strain, work and modulus. These are used as reference values in the following regression models. Prior to modeling all four replicates are averaged across the sample/object mode, and thus the $64 \times 128 \times 128$ FFT data array is reduced to a $14 \times 128 \times 128$ array. It is interesting to look at relations between FFT-feature arrays derived from these images and the corresponding rheological properties. To predict these properties, two kinds of calibration models are tried out: strong N-PLS on the $14 \times 128 \times 128$ three-way array, and weak unfold-PLS on the appropriate 14×16384 two-way array. Mean centering was performed, but no scaling was used as it was found to down-weigh the influences of important frequency components.

Calibration results using unfold-PLS and N-PLS are shown in Table 2. It is gratifying that the rheological properties can be well related to the microscopic images by means of multi-way modeling. Both unfold-PLS and N-PLS models can be established for predicting *fracture stress*, *strain*, *work* and *modulus*. Unfortunately, *facture strain* seems difficult to predict in this way. As can be seen from the comparative modeling results, N-PLS models are distinctly superior to unfold-PLS in predictions of all these rheological properties. For instance, unfold-PLS gives a model in predicting *fracture stress* with Corr. Coeff. = 0.78, RMSEP = 13921, while N-PLS provides a much better model with Corr.Coeff. = 0.91, RMSEP = 8321.

Table 2
Comparative modeling results for rheological properties, using unfold-PLS and N-PLS

Calibration methods	Rheological properties	Corr.Coeff.	RMSEP	No. of factors
Unfold-PLS	Fracture stress	0.7750	13,921	2
	Fracture strain	×	×	×
	Fracture work	0.8149	4783	2
	Modulus	0.6916	47,499	2
N-PLS	Fracture stress	0.9125	8321	4
	Fracture strain	×	×	×
	Fracture work	0.9141	3036	2
	Modulus	0.9138	21,584	3

Fracture strain cannot be predicted. All samples are kept in modeling with no outliers. Modeling parameters: Correlation Coefficient (Corr.Coeff.), Root Mean Square Error of Prediction (RMSEP) and number of factors are shown.

Table 3
Comparative percent variance captured in both *X* and *Y* by using both N-PLS and unfold-PLS in predicting the rheological property—*fracture work*

Calibration methods	*X*-block			*Y*-block		
	LV #	Fitted	Xval	Fitted	Yval	RMSEP
N-PLS	1	27.28	14.63	67.02	57.65	5060
	2	29.05	16.45	91.06	84.75	3036
	3	29.33	16.54	98.93	83.59	3149
	4	29.61	16.56	99.90	83.46	3161
	5	29.84	16.58	99.99	83.21	3186
	6	30.08	16.61	100.00	83.15	3191
Unfold-PLS	1	29.98	18.11	79.60	64.53	4987
	2	37.37	18.47	99.06	67.38	4783
	3	44.24	18.52	99.98	67.05	4807
	4	50.19	18.55	99.99	67.09	4804
	5	56.97	18.65	100.00	67.10	4803
	6	62.76	18.79	100.00	67.10	4803

Both calibration and validation variations are shown in terms of full cross-validation. LV denotes the number of latent variables, number of factors. Also shown are RMSEP values. Two components are found to be optimal in both cases.

We now try to delve into the interpretation of these N-PLS and unfold-PLS models by illustrating the calibration and full cross-validation process in prediction of one of rheological parameters. Table 3 shows percentages of variation explained in both *X* and *Y* during the calibration and full cross-validation in prediction of the property—*fracture work*. Both N-PLS and unfold-PLS give reasonably good models, but with distinctly different efforts. N-PLS fits 29.05% *X*-calibration variance, and explains 16.45% *X*-validation variance, 91.06% *Y*-calibration variance and 84.75% *Y*-validation variance with RMSEP = 3036 using two PLS-components. By contrast, unfold-PLS fits 37.37% *X*-calibration variance, and explains 18.47% *X*-validation variance, and 99.06% *Y*-calibration variance and 67.38% *Y*-validation variance with RMSEP = 4783, also by using two PLS-components. Clearly, unfold-PLS gives lower predictability and tends to overfit the models in both *X* and *Y*. For instance, it fits 37.37% *X* variation but explains only 18.47% in terms of full cross validation. The same phenomenon occurs for y variation, e.g. it fits 99.06% y variation but explains only 67.38% in terms of full cross validation.

Such overfits most likely give rise to misleading model parameters and hence to an overly optimistic interpretation of the model. On the contrary, the N-PLS model appears more parsimonious and sensible though it also displays a minor degree of overfit of X and y. It describes a little less X variation but more y variation than unfold-PLS as shown in Table 3, and gives lower RMSEP indicating higher predictability.

7.3. Evaluation

In this application (domain-transformed "multiple imagery"), the strong multi-way methods show several distinct advantages over the weak multi-way methods–unfolding methods. This is essentially because strong multi-way methods are more parsimonious, with specific use of the three-way structure in the modeling. The trilinear models are more restricted than unfolding models [12]. This leads to the fact that the fit of a trilinear model is lower than the fit of a corresponding bilinear model. Conversely, unfolding may risk taking away some three-way information and fitting more noise to the structural model. N-PLS gives better prediction results of rheological properties than unfold-PLS.

8. Discussion and conclusions

It should be underlined that a priori knowledge of the data problem (and the data background) and the appropriate problem formulation is imperative. Strong multi-way methods have many advantages over unfold methods in many senses. But it may not be universally true that they will work better than unfold methods on any and all three-way data arrays. For instance, MIA based on unfold-PCA is very suited for exploration and classification purposes as shown in application I. Applying different multi-way methods is intimately connected with proper data configuration and pertinent problem formulation. We have particularly focused on applying strong multi-way methods on both conventional **OOV** and transformed **OVV** image data array, since MIA/MIR has proven successful on **OOV** three-way image array. We have also tried to apply multi-way methods directly on raw **OOO** image arrays. As expected, no models could be obtained directly in this latter case. It is possible that for some purposes strong multi-way methods (e.g. PARAFAC) might not work well on **OOV** three-way image array, i.e. multispectral images in our application I. Esbensen [10] has pointed out that there is a phenomenological barrier between strong three-way data analysis and multivariate image analysis using unfold methods. At the moment, it may be stated very generally that strong multi-way methods are more suitable for **OVV** data array, and unfold methods (e.g. MIA) better suited for **OOV** data array in image analysis.

In applications I, II and III, we have *deliberately* crossed over this demarcation, that is to say, both unfold-PCA and strong three-way methods have been applied to **OOV**/**OVV** image arrays. Whether and when to apply MIA or strong three-way analysis on **OOV**/**OVV** image data array varies from example to example. Many points still remain open to further discourse however, but we hope that some insight into the *proper* problem-specific use of these two dichotomous approaches has been gained. Follow-up expositions and synthesizing discussions on these issues will also be presented in a sequel paper.

Acknowledgements

The authors gratefully acknowledge Prof. Rasmus Bro, at Royal Veterinary and Agriculture University, Denmark, for helpful comments and suggestions to an earlier version of this paper. ERDAS, Atlanta supplied the original Mobile Bay multivariate image to K.H.E, greatly appreciated.

References

[1] R.C. Gonzalez, R.E. Woods, Digital Image Processing, Addison-Wesley Publishing, MA, 1993.
[2] K.H. Esbensen, S. Wold, P. Geladi, Relationships between higher-order data array configurations and problem formulations in multivariate data analysis, Journal of Chemometrics 3 (1988) 33–48.
[3] P. Geladi, H. Grahn, Multivariate Image Analysis, Wiley, England, 1996.
[4] K.H. Esbensen, P. Geladi, Strategy of Multivariate Image Analysis (MIA), Chemometrics and Intelligent Laboratory Systems 7 (1989) 67–86.
[5] K.H. Esbensen, P. Geladi, H. Grahn, Strategies for multivariate image regression, Chemometrics and Intelligent Laboratory Systems 14 (1992) 357–374.

[6] P. Geladi, et al., Principal component analysis of multivariate images, Chemometrics and Intelligent Laboratory Systems 5 (1989) 209–220.
[7] P. Geladi, K.H. Esbensen, Regression on multivariate images: principal component regression for modeling, prediction and visual diagnostical tools, Journal of Chemometrics 5 (1991) 97–111.
[8] J.P. Wold, K. Kvaal, B. Egelandsdal, Quantification of intramuscular fat content in beef by combining autofluorescence spectra and autofluorescence images, Applied Spectroscopy 53 (4) (1999).
[9] J.P. Wold, Rapid quality assessment of meat and fish by using near-infrared spectroscopy autofluorescence spectroscopy and image analysis. PhD thesis. Agricultural University of Norway, 2000.
[10] T.T. Lied, P. Geladi, K.H. Esbensen, Multivariate image regression (MIR): implementation of image PLSR-first forays, Journal of Chemometrics 14 (2000) 585–598.
[11] B. Wise, R. Bro, "N-way Analysis" course in CAC-2000. Antwerp, 2000.
[12] R. Bro, Multi-way analysis in the food industry. Doctoral thesis. Royal Veterinary and Agricultural University, Denmark, 1998.
[13] R. Bro, PARAFAC. Tutorial and applications, Chemometrics and Intelligent Laboratory Systems 38 (1997) 149–171.
[14] R. Bro, Multi-way calibration. Multilear PLS, Journal of Chemometrics 10 (1996) 47–61.
[15] A.K. Smilde, Comments on multilinear PLS, Journal of Chemometrics 11 (1997) 367–377.
[16] C.A. Andersson, R. Bro, Interactive course for *N*-way analysis, Royal Veterinary and Agricultural University, Denmark. URL: http://www.models.kvl.dk/.
[17] C.A. Andersson, R. Bro, The *N*-way toolbox for Matlab, Royal Veterinary and Agricultural University, Denmark. URL: http://www.models.kvl.dk/source/.
[18] J. Huang, K.H. Esbensen, Applications of AMT (Angle Measure Technique) in image analysis: Part I. A new methodology for in-situ powder characterization, Chemometrics and Intelligent Laboratory Systems 54 (2000) 1–19.
[19] J. Huang, K.H. Esbensen, Applications of AMT (Angle Measure Technique) in image analysis: Part II. Prediction of powder functional properties and mixing components using Multivariate AMT Regression (MAR), Chemometrics and Intelligent Laboratory Systems 57 (2001) 37–56.
[20] R. Bro, A.K. Smilde, Centering and scaling in component analysis, Journal of Chemometrics 17 (2003) 16–33.